Physica Medica 141 (2026) 105709

Contents lists available at ScienceDirect

Physica Medica

journal homepage: www.elsevier.com/locate/ejmp

Original paper

# Enhancing total skin electron therapy: Introducing rotational technique and in-house-built flattening filter

Livia Marrazzo [a,b,*], Gabriele Simontacchi [c], Danial Seifi [d], Deborah Chilà [a], Andrea Lastrucci [e], Andrea Profili [f], Silvia Calusi [b], Marta Casati [b], Margherita Zani [b], Chiara Arilli [b], Antonella Compagnucci [b], Cinzia Talamonti [a,b], Lorenzo Livi [a,c], Stefania Pallotta [a,b]

[a] University of Florence, Department of Experimental and Clinical Biomedical Sciences "Mario Serio", Firenze, Italy
[b] Careggi University Hospital, Medical Physics Unit, Firenze, Italy
[c] Careggi University Hospital, Radiation Oncology Unit, Firenze, Italy
[d] Department of Medical Physics, Faculty of Medicine, Mazandaran University of Medical Sciences, Sari, Iran
[e] Department of Allied Health Professions, Azienda Ospedaliero-Universitaria Careggi, 50134 Florence, Italy
[f] University of Florence, Department of Industrial Engineering, Italy

ARTICLE INFO

*Keywords:*
Total Skin Electron Therapy
Rotational technique
End-to-end test

ABSTRACT

*Purpose:* To implement and commission a rotational Total Skin Electron Therapy (TSET) technique using high-dose-rate electron (HDRE) beams on an Elekta VersaHD linac and a custom-made flattening filter (FF), with the aim of improving delivery efficiency and dose uniformity.
*Methods:* Two HDRE beams (6 and 8 MeV) were characterized at an extended source-to-skin distance (SSD = 490 cm) using EBT3 film dosimetry. A customized FF was designed to optimize field uniformity in both vertical and horizontal directions. Percentage depth dose (PDD) and profile measurements were acquired in static and rotational setups. Monte Carlo simulations with EGSnrc/BEAMnrc and DOSXYZnrc were used to model the linac head and validated against measurements. Output ratios (ORs) were measured on a phantom to estimate the monitor units needed for rotational delivery. End-to-end (E2E) testing with an Alderson-Rando phantom and in vivo dosimetry on the first 50 patients were performed to assess dose uniformity and reproducibility.
*Results:* The custom FF significantly improved field flatness. Measured surface doses per 1000 MU were 82 cGy (HDRE1) and 106 cGy (HDRE2), with ORs of 0.52 and 0.56, respectively. The rotational technique allowed dose rates of 12.8–17.9 cGy/min and treatment times of 6–8 min. PDDs from Monte Carlo simulations matched measurements. E2E and in vivo dosimetry confirmed high uniformity and <1 % variability. In vivo dosimetry confirmed adequate surface dose coverage and intra-patient consistency.
*Conclusions:* The rotational TSET technique using HDRE beams on a VersaHD linac with a custom FF is feasible, reproducible, and dosimetrically robust, representing a valid alternative to conventional dual-field approaches.

## 1. Introduction

Total Skin Electron Therapy (TSET) is a technique aiming at the irradiation of the whole skin, introduced for the treatment of mycosis fungoides, the most common subtype of primary cutaneous T-cell lymphoma [1–4]. TSET was first implemented with a linear accelerator at Stanford University [5] in the 1950s. It is a complex technique that requires a strong collaboration of a dedicated multi professional team, involving physicists, radiation therapists and radiation oncologists [2,6]. The primary goal of this irradiation technique is to achieve complete or partial remission while minimizing toxicity. To achieve this, it is essential to deliver a specific dose evenly over the entire surface of the skin to a precise depth [3,7]. Several technical solutions have been developed during the years to achieve the hard task of a homogeneous irradiation of the skin [1,7,8]. Since large fields are required, treatment is generally performed at a Source to Surface Distance (SSD) much larger

* Corresponding author at: Department of Experimental and Clinical Biomedical Sciences "M. Serio", University of Florence, Viale Morgagni 50, 501340 Florence, Italy.
*E-mail address:* livia.marrazzo@unifi.it (L. Marrazzo).

https://doi.org/10.1016/j.ejmp.2025.105709
Received 16 June 2025; Received in revised form 4 December 2025; Accepted 12 December 2025
Available online 16 December 2025

than the isocenter distance; high electron dose rates (HDRE) at isocenter are used to minimize treatment time.

A high average linac beam current is needed to provide an adequately high dose rate in the patient treatment plane several meters distant. Dose rates at the patient of 1 Gy/min or higher (not lower than 0.25 Gy/min at Dmax, the dose maximum) are desirable in order to reduce treatment times and thus minimize patient motion and fatigue [1].

Employed energies are 3–7 MeV at the patient surface and 4–10 MeV at the accelerator beam exit window [1]. A beam degrader (spoiler) is usually placed between the electron source and the patient to reduce the initial electron energy [9–11]. Energy is chosen depending on clinical needs and lymphomas cell infiltration depth and usually should range from 4 MeV to 8 MeV [7,12]. Nowadays the most common procedure used is called Stanford six dual-field method [1,7,11,13]. This technique involves the use of multiple angled beams directed toward a standing patient. Each dual field is composed by a pair of angled beams: one directed toward the inferior part of the patient and the other one toward the superior part. The two adjacent fields are required to cover the full vertical extent of the patient, since the maximum field size at the treatment SSD is insufficient for whole-body coverage with a single beam [5,7,12]. Because of superposition. When both profiles are added together, an almost homogeneous profile is created [14].

The patient stands on a platform and dual fields are delivered for six patient's positions/orientations (60° step), also corresponding to different patient's positions, including anterior, posterior, right posterior oblique, left posterior oblique, left anterior oblique, and right anterior oblique [1,12,15]. A complete treatment fraction is often delivered in two days, by alternating sets of complementary patients' positions [15,16].

Such a technique is extremely demanding. Firstly, it is very time-consuming [17,18], as patients have to stand motionless for 10 to 30 min during the treatment, which is particularly difficult for elderly and weak patients. Secondly, the achievable dose homogeneity on the patient surface is limited by the inaccuracies due to patient positioning and fields overlapping, so that the complexity of the junctional dose calculation should be considered with caution [9]. Moreover, the intra-fraction dose homogeneity cannot be guaranteed and the daily delivered dose is highly inhomogeneous.

In our Institution we have been treating patients for the last 13 years by using a six dual fields technique. We recently decided to move, inspired by the work of Reynard [19] and taking advantage of the installation of a new linac, to a new rotational technique with the aim of improving patient dose homogeneity, patient comfort and treatment delivery. A specifically designed flattening filter was manufactured to avoid the necessity for a dual field, enabling a single-field solution while maintaining adequate dose uniformity.

The aim of this work is to describe the main steps involved in the implementation of the technique as well as the development and characterization of the filter.

A Monte Carlo (MC) simulation was performed to model the linac head, flattening filter, and treatment geometry. The simulation was validated by comparing the simulated and measured percentage depth doses (PDDs) and lateral dose profiles, both with and without the filter at the treatment SSD. Once validated, the MC simulation was used to calculate PDDs and lateral dose profiles at various SSDs. The primary goal of the simulation was to enable the evaluation of new filter configurations or SSD values while minimizing the need for extensive physical measurements.

In addition, in vivo dosimetry using GAFCHROMIC® EBT3 films was implemented to measure the dose distribution along the patient's waistline, in order to assess treatment homogeneity and compare it with a standard dual-field technique.

This study presents the implementation process, filter development and characterization, MC simulation validation, and clinical dosimetric results.

## 2. Materials and methods

TSET was implemented using an Elekta VersaHD linear accelerator (Elekta AB, Stockholm, Sweden), which has the capability of producing high-dose-rate electron (HDRE) beams with nominal energies of 6 MeV and 8 MeV. HDRE delivery is activated by a key mechanism.

A dummy applicator must be mounted on the treatment head to bypass the linac interlock. This applicator does not collimate the beam, resulting in a field size of 40 × 40 $cm^2$ at the isocenter.

### 2.1. Rotating platform and flattening filter

A rotating platform, capable of variable-speed rotation, was designed and manufactured. Various configurations of the flattening filter were tested to optimize beam homogeneity and select the most appropriate beam penetration based on clinical requirements, as well as different SSDs. The flattening filter was introduced to eliminate the need for a dual field. Percentage Depth Doses (PDDs) for both static and rotational beams were measured using radiochromic GafChromic® EBT3 films (Ashland Inc., Wayne, NJ) in the setup illustrated in Fig. 1 (a). Strips of films were placed on a horizontal plane at isocenter level within a cylindrical Virtual Water™ phantom (Gammex RMI, Middleton, WI), also known as the "Cheese" phantom. The phantom has a diameter of 30 cm and a length of 18 cm.

EBT3 films were digitized with an Epson Expression 10000XL scanner in transmission mode. RGB positive images were captured at 16-bit depth per color channel with a spatial resolution of 72 dpi (pixel size 339 μm). Scanning was performed using the Epson Scan driver with all color correction options disabled. The films were always placed on the scanner plate in landscape orientation and evaluation was consistently performed 24 h after irradiation.

The transmission images were saved in TIFF format. A previously determined calibration curve (specific to the same film lot) was applied. To convert the film pixel values into dose, a multi-channel method was employed. Details on film calibration and handling can be found in [20]. For film calibration, dose conversion, and PDDs and profile extraction, FilmQA™ Pro software (Ashland Inc., Wayne, NJ) was used.

To evaluate the effectiveness of the flattening filter in reducing beam inhomogeneity, horizontal and vertical profiles, with and without the filter, were measured using GAFCHROMIC® EBT3 films cut into strips and attached to a PMMA panel.

### 2.2. Technique commissioning

Both available electron energies were tested and commissioned. The data for HDRE2 are provided in the Supplementary Material, while the main focus of this study is on HDRE1, which is expected to be more widely used in clinical practice. The optimal combination of parameters (SSD and flattening filter composition) was defined through a series of measurements and a trial-and-error process carried out in collaboration with a radiation oncologist. The intermediate measurements leading to this configuration cannot be presented in detail here. After selecting the optimal parameters, the commissioning phase included the following steps:

- The absolute output for the two static electron energies, using the custom flattening filter, was measured with an Advanced Markus parallel-plate ionization chamber (PTW, Freiburg, Germany), following the IAEA TRS-398 Code of Practice [21]. The chamber was placed in a PMMA phantom at the selected SSD for treatment, at the depth of maximum dose, with the gantry at 270 degrees, the collimator set to 40 cm × 40 cm and rotated to 45 degrees, and the custom flattening filter in place.
- The monitor units (MUs) required for delivery on a rotating patient were determined by measuring, in the Cheese phantom, the output ratio (OR) between static and rotational outputs. This was done using

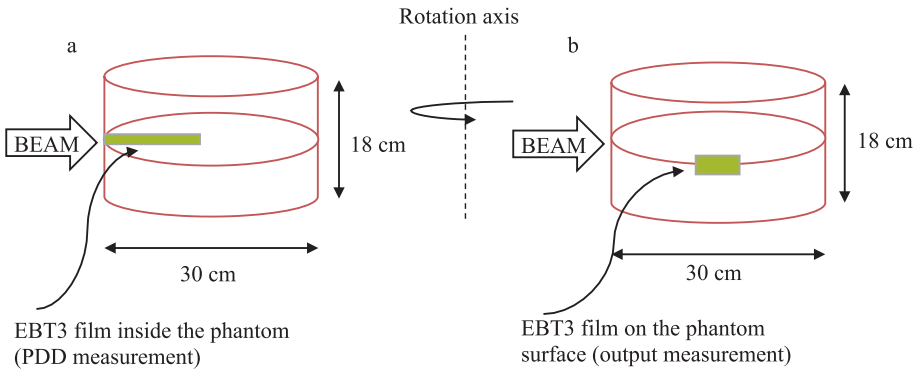


**Fig. 1.** Schematic of the experimental setup for measuring Percentage Depth Dose (PDD) (a) and output (b) for both static and rotational beams.

EBT3 films placed on the phantom surface for the static output, and with the phantom rotating for the rotational output (Fig. 1, b).

$$OutputRatio(OR) = \frac{RotationalOutput}{StaticOutput} \quad (1)$$

$$RotationalMUs = \frac{StaticMUs}{OR} \quad (2)$$

- An end-to-end test was performed using the Alderson Rando anthropomorphic phantom (Alderson Research Laboratories, Stanford, CT) and repeated twice to verify repeatability.

### 2.3. Monte Carlo simulation

A Monte Carlo (MC) simulation was performed to model the linac head, flattening filter, and treatment geometry. Source parameters (initial energy, full width half maximum, and angular spread) were adjusted to match the simulated results with measured percentage depth doses (PDDs) and lateral dose profiles, both with and without the filter at the treatment SSD. Once validated, the MC simulation was used to calculate PDDs and lateral dose profiles at various SSDs. The primary goal of the simulation was to enable the evaluation of new treatment configurations (i.e. different SSD) while minimizing the need for extensive physical measurements.

#### 2.3.1. Accelerator treatment head modelling

The Elekta Versa HD accelerator treatment head for the 6 MeV beam at an SSD of 490 cm was simulated using EGSnrc/BEAMnrc [22]. This software was chosen for its simplicity in modelling medical linear accelerators. Simulations were run on a Windows 10 system using an Intel Xeon Gold 6138 CPU with 40 cores, 80 threads, and 96 GB of RAM.

The simulation began with electrons emitted from the vacuum window of the linac head.

The Elekta Versa HD accelerator head geometry was not directly available in the EGSnrc/BEAMnrc libraries; therefore, an in-house BEAMnrc model was reconstructed based on publicly available technical specifications and commissioning data of the accelerator. No proprietary or confidential information from the manufacturer was used or obtained. Component modules (CMs) in BEAMnrc were used to simulate the main elements: scattering foils, monitor chamber, jaws, and multi-leaf collimator. For the 6 MeV beam, no primary scattering foil was used; the beam was broadened by the secondary foil. The electron source, modelled as a mono-energetic Gaussian beam, had an initial energy of 6.64 MeV as per the manufacturer's specifications. Each CM was assigned a LATCH bit to track particle interactions throughout the simulation. Key parameters included ECUT (electron kinetic-energy cutoff) = 0.521 MeV, PCUT (photon cutoff) = 0.01 MeV, with standard global SMAX (maximum geometric step) and ESTEPE (maximum fractional energy loss per step) values of 5.0 cm and 0.25, respectively. The boundary crossing method was designated as PRESTA-I, while the electron transport step algorithm was referred to as PRESTA-II.

#### 2.3.2. Dose calculations

The accelerator model was linked to the DOSXYZnrc user code [23] to calculate dose distributions in a water phantom, eliminating the need for intermediate phase-space data storage. The model was validated by comparing the measured PDD curves with those generated by DOSXYZnrc. Fine-tuning of the model was performed by adjusting electron source energy, FWHM, and adding a mean angular spread.

Each simulation was run using two billion histories, with 80 processors in parallel. Directional bremsstrahlung splitting (DBS) was employed to reduce simulation time. To achieve a dose uncertainty of less than 1 %, 9 billion histories were simulated for each dose calculation.

### 2.4. In-vivo dosimetry

In-vivo dosimetry was performed on the first 50 treated patients using EBT3 films placed on the abdomen and back. For the first three patients, measurements were acquired twice (on consecutive fractions) to assess intra-patient repeatability, while for the remaining, dosimetry was conducted once during the first fraction. To evaluate the advantage of the rotational technique in terms of dose homogeneity compared to the six-dual-field technique, the distribution of the differences between anterior and posterior doses was analysed for the 50 treated patients and compared with that of 112 patients treated with the static approach.

Furthermore, dose homogeneity along the patient's waistline was assessed using a belt of radiochromic film and compared with the distribution achieved using the six-dual field technique.

Additional in vivo measurements were performed at other body sites, but we chose to report only the extremities (wrist and ankles), as they are of particular interest.

## 3. Results

### 3.1. Rotating platform and flattening filter

The rotating platform has a circular standing area with a diameter of 100 cm, and its top surface is 23 cm above the floor. The distance from the isocenter to the floor is 125 cm, making the distance from the platform's surface to the isocenter 102 cm. The platform is equipped with a variable-speed motor that allows rotational rates between 0.5 and 10 rpm, controlled by adjusting the input current. A speed of 3 rpm was chosen as a balance between patient comfort and the number of rotations needed to ensure dosimetric consistency regardless of start and stop positions.

To help patients maintain their balance during rotational treatment, a suspended rotating handlebar is positioned midair above the axis of rotation. Patients hold onto the handle with one arm during treatment,

alternating arms in subsequent sessions.

The SSD was set to 490 cm for both energies, though an SSD of 390 cm was also tested (data not shown). An SSD of 490 cm was chosen as a compromise between field size and dose rate. The value results from the platform geometry, with its center at 500 cm from the source, corresponding to ~490 cm at the patient surface.

To achieve the maximum field size, the TSET technique was delivered with the gantry positioned laterally at 270 degrees and the collimator at 45 degrees, thus maximizing the vertical and horizontal field axes.

A flattening filter configuration consisting of layers of PMMA, lead (thickness 0.1 mm, diameter 220 mm), and aluminium (thickness 1.6 mm, diameter 70 mm) was selected, similar to the one described in [18], but with thinner PMMA layers (2 × 0.4 cm instead of 2 × 0.8 cm). The composition of the flattening filter, shown in cross-section and front view in Fig. 2a, includes trimmed upper and lower 10 mm sections of the lead disc, which preferentially attenuates the central 'hot' part of the beam, as suggested in [19], to increase the relative fluence at the superior and inferior field regions and achieve a more uniform vertical profile. To ensure rigidity, the two metallic discs are secured between two PMMA plates, with portions of the plates removed to further increase fluence at the field's upper and lower regions.

To attach the filter to the accelerator head and bypass the interlock, it was mounted on the dummy applicator, as shown in Fig. 2b and Fig. 3.

Fig. 4 shows the static and rotational PDDs for HDRE1 (data for HDRE2 are reported in Supplementary Fig. 1).

The static PDD corresponds to measurements with the phantom at rest and the beam orthogonal to its surface. In the rotational setup (either continuously on the rotating platform or stepwise in the Stanford-like technique), the beam enters the "Cheese" phantom at oblique angles, effectively increasing the path length to the central axis where the PDD film is located. As a result, the mean electron energy decreases and R100 shifts toward the surface, reflecting a softer energy spectrum.

Table 1 summarizes the key beam quality parameters derived from the PDD curves for the HDRE1, in both static and rotational modes: R100 (depth of maximum dose), R50 (depth at 50 % of maximum dose), and Rp (practical range) are standard descriptors of electron beam penetration used for beam commissioning. From R50, the most probable surface energy (Ep0) and the mean energy at the phantom surface (E0mean) can be calculated [1], providing information on the effective electron energy. Finally, the "Bremsstrahlung background (%)" – X-ray Bck. (%) – quantifies the fraction of penetrating X-ray contamination present in the beam. Since TSET aims to confine the dose to superficial tissues, minimizing this component is particularly important to avoid unwanted dose at depth. Definitions and the relationships between these quantities are provided in [1]. Data for HDRE2 are reported in Supplementary Table 1.

Fig. 5 shows a comparison of vertical profiles, with and without the filter, for the 6 MeV HDRE beam at an SSD of 490 cm. The lines represent interpolations of experimental data to reduce measurement noise. Without the FF, the dose at ±1000 mm from the central axis is approximately 69 % of the central axis dose, compared to a 93 % with the filter. With the filter in place, the 95 % dose level spans a length of 168 cm, while the 90 % dose level extends to about 232 cm.

### 3.2. Technique commissioning

Both beam energies were calibrated following the IAEA TRS-398 [21] protocol to deliver 1 cGy per MU at an SSD of 100 cm, with the dummy applicator in place and without a customized flattening filter. The absorbed dose delivered per 1000 MU on the central axis at an SSD of 490 cm was measured as 82 cGy for HDRE1 and 106 cGy for HDRE2 (static beams). Using equation (1), the output ratio (OR) was found to be 0.52 for HDRE1 and 0.56 for HDRE2. Consequently, based on equation (2), the monitor units required to deliver 100 cGy were calculated as 2345 for HDRE1 and 1679 for HDRE2. This corresponds to surface dose rates of 12.8 cGy/min and 17.9 cGy/min for HDRE1 and HDRE2, respectively.

A dose of 1 Gy at the patient's surface is delivered in approximately 8 min for HDRE1 and 6 min for HDRE2, corresponding to roughly 24 and 18 full rotations, respectively. For TSET patients, the prescription dose and fractionation are defined according to the clinical setting and the purpose of treatment: common prescriptions range from 12 Gy delivered in 12 fractions (1 Gy per fraction) or 8 fractions (1.5 Gy per fraction) for low-dose TSET to 20–36 Gy at 1 Gy per fraction when higher doses are required.

Fig. 6 presents the dose map measured at the abdomen level of the Alderson Rando phantom, along with a photograph of the phantom on the rotating platform. The end-to-end (E2E) test showed excellent dose uniformity across the phantom (superficial dose: 1 Gy ± 2 %) and high delivery reproducibility (<1%).

### 3.3. Monte Carlo simulation

#### 3.3.1. Comparison with measurements

The comparison between the MC simulation and the experimental measurements reveals a favourable agreement, supporting the accuracy and reliability of the simulation model (Fig. 7). The dose distribution as a function of depth shows that the MC-generated curve closely follows the experimental trend, particularly in build-up region where the therapeutic dose is typically delivered (Fig. 7a). At shallow depths (0–5 mm), the MC simulation (0.820 at 0 mm, 0.991 at 5 mm) closely matches experimental measurements (0.840 at 0 mm, 0.998 at 5 mm),

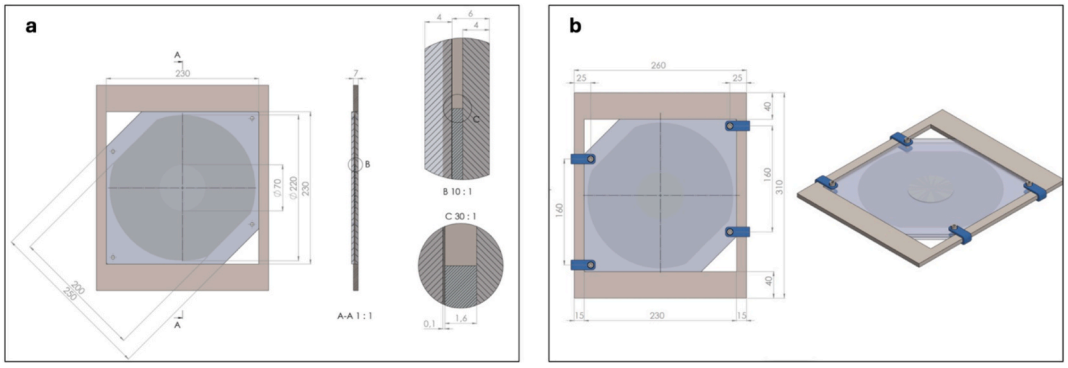


**Fig. 2.** a) Flattening filter composition shown in cross-section and front view. the dummy applicator frame is beige, the PMMA layer is light blue (hatched in cross section view), the cut disk in grey represents the lead layer (fine hatched in cross section view, and the central light grey disk corresponds to aluminium (solid in cross section view). b) Flattening filter mounted on the dummy applicator using 3D-printed clips. All measurements are given in mm. (For interpretation of the references to colour in this figure legend, the reader is referred to the web version of this article.)

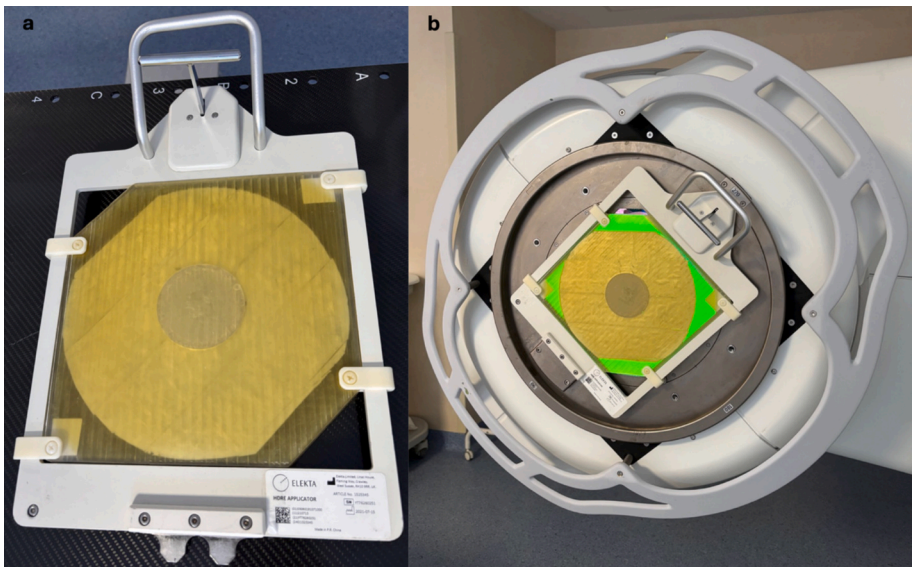


**Fig. 3.** a) The flattening filter attached to the dummy applicator; b) Dummy applicator with flattening filter applied to the linac head.

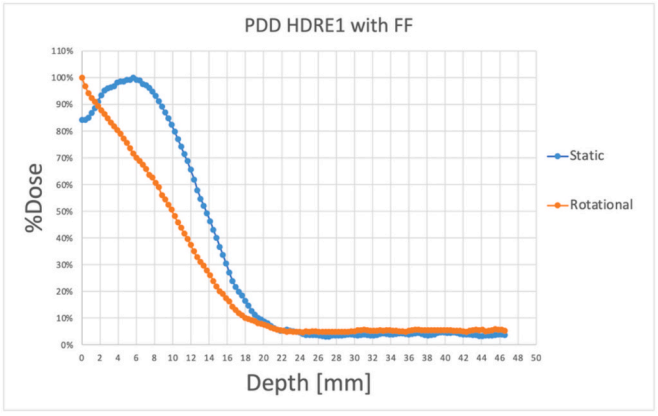


**Fig. 4.** Static and rotational PDDs for the HDRE1 (6 MeV).

with differences less than 1 %.

In Fig. 7b the comparison between MC simulation and measurement for vertical profiles (with and without FF) is shown. Again, MC-generated curve closely follows the experimental data.

### 3.3.2. *PDD and profile variations with SSD*

Once validated, the Monte Carlo (MC) simulation was used to compute PDDs and lateral dose profiles at various SSDs. For vertical profiles, at an SSD of 390 cm, the 95 % dose level spans a length of 136 cm, while the 90 % dose level extends to 184 cm (with a minimum value of 88 % at ±100 cm). When the SSD is further reduced to 290 cm, the 95 % dose level covers 104 cm, and the 90 % dose level covers 152 cm (with a minimum value of 83 % at ±100 cm).

Calculated vertical profiles with and without FF are shown in Supplementary Fig. 2.

Regarding PDDs, the curves for SSDs of 490 cm, 390 cm, and 290 cm are very similar and substantially overlap (see Supplementary Fig. 3).

### 3.4. *In-vivo dosimetry*

We started treating patients in December 2022. The results for the in-vivo dosimetry for the first 50 patients, treated over a two-year period, are reported in Supplementary Fig. 4.

Approximately 25 TSET patients are treated annually in our center, out of a total of about 2500 patients. The technique is routinely delivered on one of four twin linacs and was also commissioned on a second linac used as backup.

The average measured value is (99 ± 4) cGy. Intra-patient variation is within 2.5 %. The mean values measured on the abdomen and the back are (100 ± 5) cGy and (99 ± 6) cGy, respectively (*t*-test p-value 0.1), thus confirming the optimal dose homogeneity along the patient waist. The maximum discrepancy was found for an overweight patient (12 %).

In Fig. 8 the distributions of the differences between anterior and posterior doses are reported for the static (a) and the rotational approach (b). In the static approach differences up to 30 % can be observed, while in the rotational most of the differences are within 10 %.

With the static approach, 37 % of the differences between anterior and posterior measured doses are within 5 %, 20 % fall between 5 % and 10 %, 31 % between 10 % and 20 %, and 10 % exceed 30 %. In contrast, with the rotational technique, 62 % of the differences are within 5 %, 33 % fall between 5 % and 10 %, 5 % between 10 % and 20 %, and none exceed 30 %.

Fig. 9 reports dose profiles measured with an EBT3 film "belt" positioned around the patient's waistline, comparing the rotational technique with the six-dual-field approach in two representative cases. The results highlight that the rotational technique achieves a more uniform dose distribution, contributing to better intra-fraction dose homogeneity.

**Table 1**
Static and rotational R100 (depth of the maximum dose), R50 (depth of the 50 % of the maximum dose), Rp (practical range), Ep0 (most probable energy at the phantom surface), E0mean (mean energy at the phantom surface) and dose due to X-rays contamination (bremsstrahlung background tail, X-Ray Bck. (%)) for HDRE1 (6 MeV).

| | | R100 (mm) | R50 (mm) | Rp (mm) | Ep0 (MeV) | E0mean (MeV) | X-Ray Bck. (%) |
|---|---|---|---|---|---|---|---|
| **HDRE1** | **Static** | 5.7 | 13.7 | 19.0 | 4.0 | 3.2 | 3.7 |
| | **Rotational** | 0.0 | 10.0 | 17.0 | 3.6 | 2.3 | 5.3 |

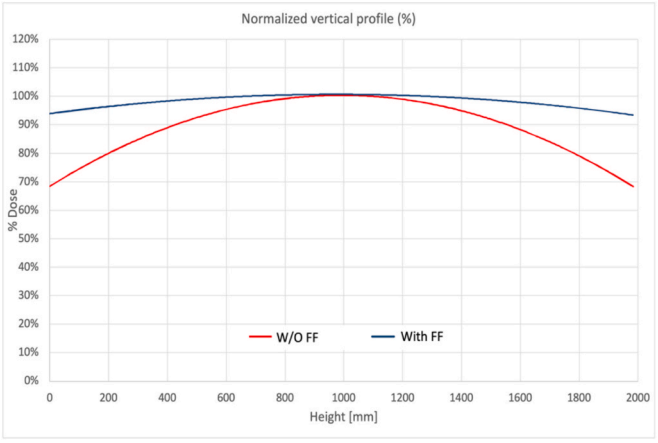


**Fig. 5.** Normalized vertical profiles with (blue) and without (red) flattening filter (FF) for the HDRE1 beam at 490 cm SSD. (For interpretation of the references to colour in this figure legend, the reader is referred to the web version of this article.)

At the extremities, the maximum underdosage was measured at the wrist for the tallest patient (93 % of the prescription), while the average value at the ankles was (102 ± 1)% of the prescription.

## 4. Discussion

The implementation of the rotational technique for TSET represents an important advancement in the treatment of the entire skin surface, as it allows for more uniform dose distribution and improved intra-fraction dose homogeneity. Our experience confirms that this technique is feasible and introduces several key improvements over traditional methods, such as the six-dual-field technique. In Table 2 a comparison between the main characteristics of the modified Stanford and the rotational TSET techniques is presented.

One of the most notable benefits of the rotational technique is its ability to achieve superior dose homogeneity across the patient's skin surface. The six-dual-field technique struggles to maintain consistent dose distribution within and between treatment sessions. Our findings indicate that the rotational approach effectively mitigates these issues by preserving intra-fraction dose homogeneity, which is important for treatment efficacy. While this may help limit acute skin toxicity commonly observed with uneven dose delivery, the impact on long-term side effects has not been directly assessed in this study.

A recent review [8] summarized eight studies on rotational TSET, highlighting its potential for improved dose homogeneity and shorter treatment times compared to the Stanford technique, while also noting the practical challenges related to the need for dedicated equipment.

A comparison with previous work further supports the advantages of the rotational approach. In a recent paper a similar end-to-end test was performed on an Alderson Rando phantom and Gafchromic films using the modified Stanford technique [14]. The reported surface dose uniformity was 3 Gy ± 15 %, with noticeable over-dosage (up to 15 %) in specific regions such as the tip of the nose, paranasal sinuses, and ears. In our phantom study, the measured surface uniformity was significantly improved, with values of 1 Gy ± 2 %, confirming the ability of the rotational technique to achieve a more homogeneous dose distribution across the patient surface.

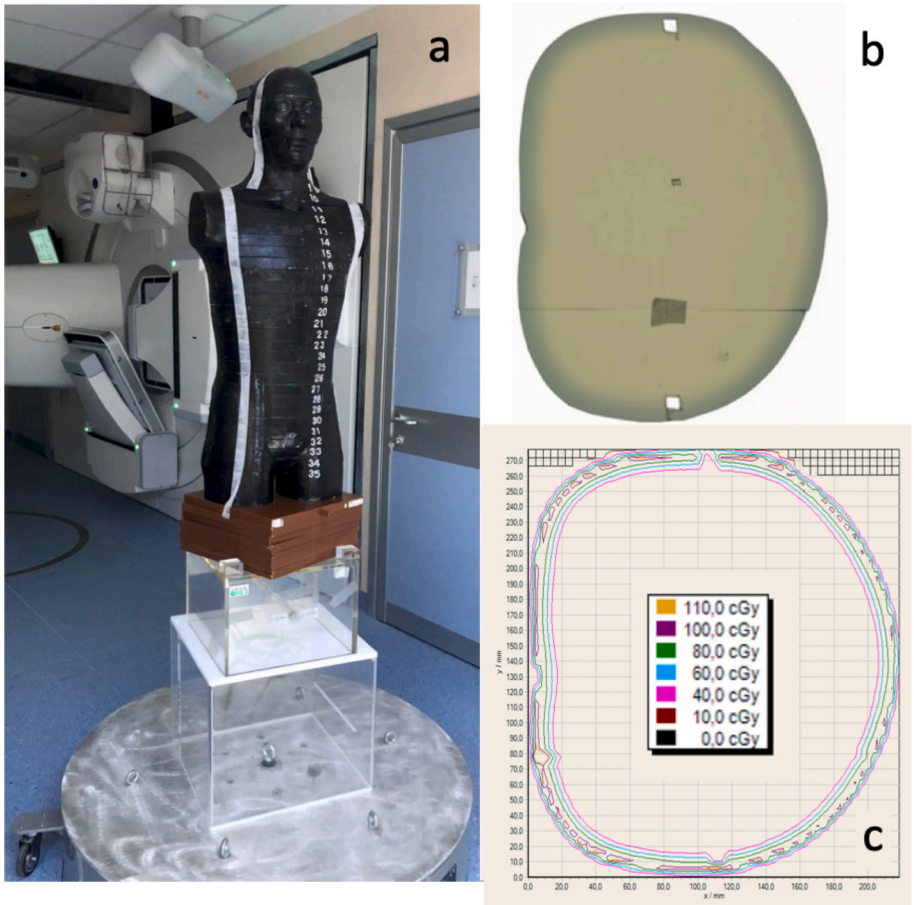


**Fig. 6.** a) Alderson Rando phantom used for the end-to-end test placed on the rotating platform. b) EBT3 film placed between two Alderson Rando slices at the level of abdomen. c) Dose maps measured with EBT3 within the phantom (6 MeV, SSD=490cm).

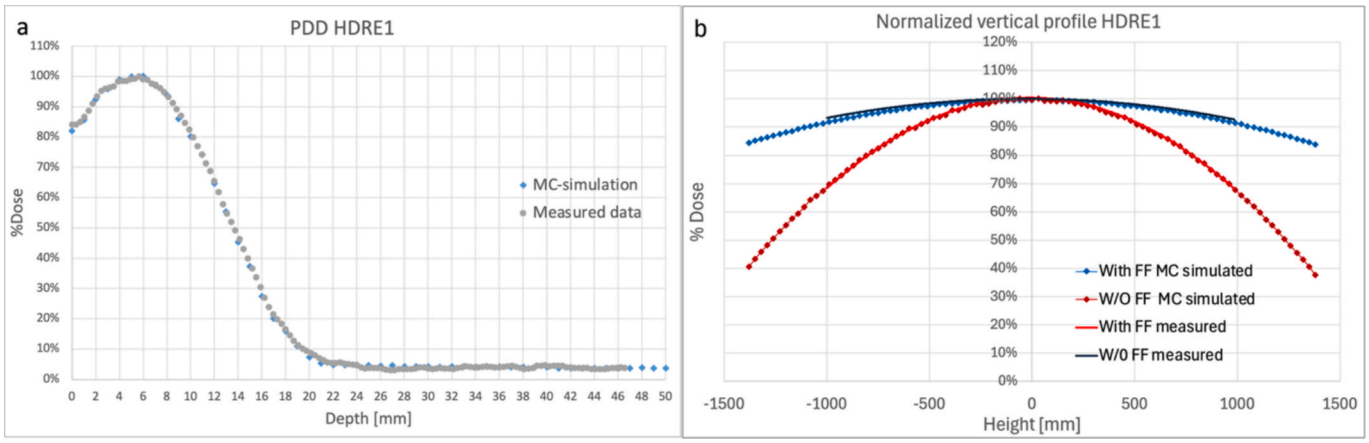


**Fig. 7.** a) Comparison between MC simulation and measurement for HDRE1 PDD. b) Comparison between MC simulation and measurement for HDRE1 vertical profiles with and without FF.

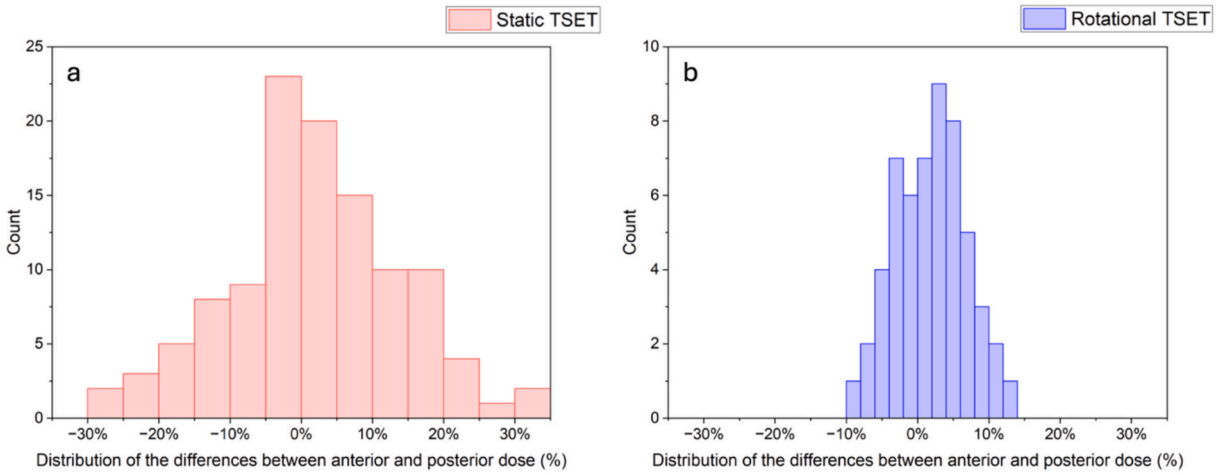


**Fig. 8.** Distributions of the differences between anterior and posterior doses are reported for the static (a) and the rotational approach (b).

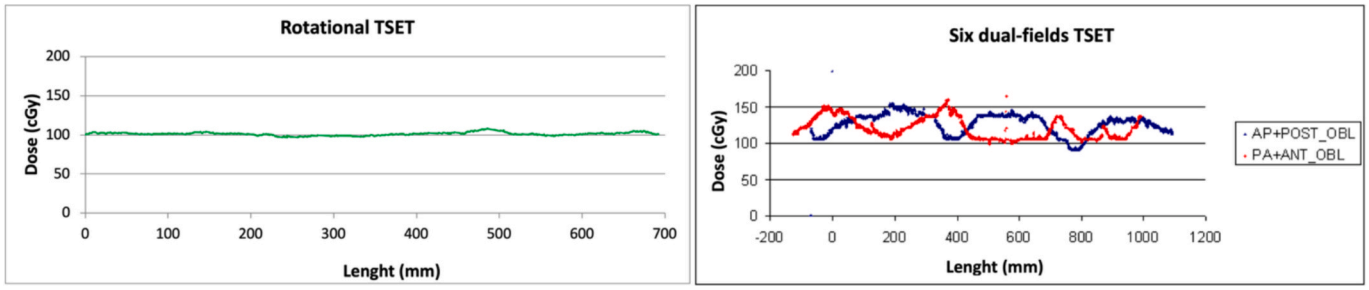


**Fig. 9.** Dose profiles extracted from an EBT3 film "belt" along the patient's waistline. The rotational technique is shown in green, while the six-dual-field technique is represented by blue (first fraction: one anterior and two oblique posterior fields) and red (second fraction: one posterior and two oblique anterior fields). (For interpretation of the references to colour in this figure legend, the reader is referred to the web version of this article.)

Moreover, the introduction of the flattening filter allows the use a single beam to treat the entire patient surface without the need for dual fields, thereby shortening the treatment time.

Since the custom flattening filter is positioned downstream of the LINAC's transmission ionization chamber, there is a potential risk of incorrect treatment setup if the filter is not in place or if the filter breaks and shifts during treatment. This could lead to an unexpectedly high and uneven dose. To mitigate this risk, a secondary dosimetry monitoring system has been put in place. An electron diode (T60010EP-4, in-vivo electron semiconductor probe, PTW, Freiburg, Germany) connected to an electrometer (DPD6 Therados, Uppsala, Sweden) is placed on the stationary base of the rotating platform in a fixed position. During beam calibration, a relative factor specific to this setup is established with the secondary dosimetry system, allowing for consistent monitoring of daily treatments and enhancing safety.

Regarding the determination of the Output Ratio, as noted in the work by Reynard et al. [19], any point on the rotating patient remains within the radiation field for half of the rotation period and is obscured by other parts of the body during the other half. Consequently, the OR (equation (1) is expected to be close to 0.5. Our measured values – 0.52

**Table 2**
Comparison between the main characteristics of the Modified Stanford and the Rotational TSET techniques.

| Aspect | Modified Stanford TSET (6–dual–field) | Rotational TSET with FF |
|---|---|---|
| Beam modality | High dose rate electrons | High dose rate electrons |
| Equipment requirements | Large bunker, patient standing platform, spoiler | Large bunker, patient rotating platform, flattening filter |
| Gantry | Two angled positions for each beam | One horizontal beam |
| SSD | Typically, extended SSD (varies by center) | Typically, extended SSD |
| Field formation | Dual fields arranged to cover total skin | Single field with FF |
| Patient positioning | Multiple patient's positions/ orientations per day | Single patient position |
| Intrafraction dose homogeneity | Highly inhomogeneous intrafraction dose distribution | Homogeneous intrafraction dose distribution |
| Dose homogeneity (A–P differences) from in-vivo EBT3 analyses | Within 5 %: 37 %; 5–10 %: 20 %; 10–20 %: 31 %; >30 %: 10 % | Within 5 %: 62 %; 5–10 %: 33 %; 10–20 %: 5 %; >30 %: 0 % |
| Practical constraints | Room size, patient tolerance for multiple positions and slightly longer treatment times | Room size, patient tolerance for standing on a rotating platform |
| Delivery time | ≈6 − 10 min | ≈8 min (HDRE1) / ≈6 min (HDRE2) |
| Initial setup time | ≈10 min | ≈10 min |
| Intra-beam setup time | ≈5 min | N/A |

for HDRE1 and 0.56 for HDRE2 − are consistent with those reported by Reynard et al. [19] (0.443 determined using Gafchromic EBT film, and 0.448 determined using a MOSFET detector at an SSD of 380 cm) and by Podgorsak et al. [24] (0.45 measured using radiographic film and thermoluminescent dosimeters).

The rotational TSET technique was successfully integrated into our clinical practice, proving to be well-tolerated by the majority of patients. An aspect to consider with the rotational technique is that frailer patients may find it more challenging to maintain an upright position and balance on the rotating platform.

The ease of execution further supports the practicality of this approach, reducing the burden on both patients and healthcare providers and suggesting that this technique could be more widely adopted, potentially standardizing TSET practices and improving patient care on a broader scale. In particular, the reduction in treatment times is certainly beneficial for patients.

The simpler, single-position setup reduces patient coaching time and the need for intra-fraction corrections compared to the complex six-position conventional technique, improving overall workflow efficiency. While the delivery time itself and the initial setup time are comparable between the two techniques, the modified Stanford requires an additional intra-beam setup, during which the RTT must enter the room to adjust the patient's position and orientation after each dual-field delivery. In addition, the RTT must enter the bunker after every single beam, since gantry rotation cannot be performed remotely with the dummy applicator in place (estimated times are reported in Table 2).

The enhanced dose distribution achieved with rotational TSET may translate into better clinical outcomes, particularly in reducing the risk of both under- and over-treatment of certain skin regions. A maximum inhomogeneity of about 12 % was observed for one overweight patient. This limitation may be related to the highly non-cylindrical body contour, which challenges the assumption of rotational symmetry inherent to this technique. The closer proximity of the body surface at the waist of an obese patient to the source increases the dose rate, to an extent that depends on the SSD. Such patient-specific anatomical factors can impact dose uniformity and should be carefully considered when applying the rotational approach. Acknowledging these constraints is important for guiding the implementation of TSET in centers where patient body habitus may vary widely.

As far as we know, our experience represents the first implementation of rotational TSET in Italy, and our findings align with previous experiences that support the benefits of this technique [19].

Despite these advancements, it is important to acknowledge certain limitations of our study.

Because the conditions that require this type of radiotherapy are extremely rare, no commercial are systems specifically designed for TSET, necessitating in-house design and fabrication.

Our study can serve as a guide, but each center must implement its own filter design and perform site-specific measurements according to the linac, bunker characteristics, achievable SSD, and clinical beam-penetration requirements.

A formal risk analysis, such as those reported in other works [14,25], was not performed in our center prior to clinical implementation, as this is not standard practice and we currently lack direct experience with the methodology. Instead, we held several multidisciplinary meetings with radiation oncologists, medical physicists, and radiation therapists. These sessions focused on presenting the new technique, addressing concerns, and discussing potential risks and mitigation strategies. This collaborative approach enabled us to identify and manage the most relevant issues in a practical, clinically oriented manner.

A Monte Carlo simulation was also conducted as part of this study to support the evaluation of alternative filter configurations and SSD values, reducing the need for extensive physical measurements. In addition, it provides reference data for centers aiming to implement a rotational TSET technique with a flattening filter, particularly those with space constraints due to smaller bunker dimensions.

The close agreement between measurements and simulations confirms that the MC model accurately represents the beam characteristics, including the composition and thickness of the filter. This validates the use of MC simulation as a reliable tool for dosimetric evaluation in TSET. Furthermore, the model's ability to replicate the complex behaviour of electron transport through multilayer filtering systems highlights its potential for future optimization studies and individualized treatment planning.

While variations in SSD have minimal impact on PDD, they significantly affect the vertical field coverage. At an SSD of 390 cm, the 95 % dose level spans 100 cm, and the 90 % dose level extends to 151 cm (with a minimum of 89 % at ± 80 cm). When the SSD is reduced to 290 cm, the 95 % dose level covers only 60 cm, and the 90 % dose level shrinks to 90 cm (with a minimum of 79 % at ± 80 cm). These findings suggest that, for reduced SSDs, alternative filter configurations should be considered, or that combining a dual-field approach with the rotating platform may offer a viable solution.

Measured dose at the extremities − (93 ± 2) % of the prescription at the wrist and (102 ± 1) % at the ankles − are consistent with the observed dose profile and may also reflect an increased dose in the lower part of the field due to scatter radiation from the floor.

While Hensley et al. [11] reported an increased dose in the lower section of the electron field due to floor scatter in dual-field setups, this effect was not observed in our rotational single-field measurements and simulations. A likely explanation is that, in our configuration, no beam is directly directed toward the floor, thereby minimizing scatter contribution. We also note that the study by Reynard et al. [19] does not describe this effect, which is consistent with our findings.

With the idea of implementing a total skin irradiation technique using a commercial machine, attempts have been made to use Helical Tomotherapy (HT) [26,27], which in principle may offer several dosimetric and treatment advantages. However, in the few published experiences with HT, the treated patients experienced severe bone marrow suppression, even when treated to a dose relatively low of 12 Gy [28,29]. This increased toxicity likely reflects the higher total body dose delivered by photons in HT, compared with the lower dose imparted by

the limited range of electrons. Therefore, treatment with large electron fields should still be considered safer, and efforts to improve and standardize these techniques remain worthwhile.

Further optimization may be possible through advanced, less handmade filter manufacturing; this is one of the improvements we plan to implement, using 3D-printers.

## 5. Conclusion

The newly developed rotational technique has been demonstrated to be feasible and has been incorporated into our clinical practice. It is well tolerated by the majority of patients and represents a significant improvement in dose homogeneity and ease of execution at the linac compared to the six-dual field technique. The rotational technique also reduced the overall treatment time, from 30 to 35 min with the Stanford approach to 16–18 min including setup. Unlike the six-dual field technique, this method maintains intra-fraction dose homogeneity. To the best of our knowledge, ours is the first experience with rotational TSET in Italy.

## Funding

This research did not receive any specific grant from funding agencies in the public, commercial, or not-for-profit sectors.

## Declaration of competing interest

The authors declare that they have no known competing financial interests or personal relationships that could have appeared to influence the work reported in this paper.

## Acknowledgements

Authors would like to acknowledge FRO (Fondazione Radioterapia Oncologica) for their invaluable support in making this work possible, and Ladysound® Srl (Pistoia, Italy) for manufacturing the rotating platform and for their responsiveness and availability.

## Appendix A. Supplementary data

Supplementary data to this article can be found online at https://doi.org/10.1016/j.ejmp.2025.105709.

## References

[1] Total skin electron therapy : technique and dosimetry. Published for the American Association of Physicists in Medicine by the American Institute of Physics; 1988.
[2] Jones GW, Hoppe RT, Glatstein E. Electron beam treatment for cutaneous T-cell lymphoma. Hematol Oncol Clin N Am 1995;9:1057–76.
[3] Anacak Y, Arican Z, Bar-Deroma R, Tamir A, Kuten A. Total skin electron irradiation: evaluation of dose uniformity throughout the skin surface. Med Dosim 2003;28:31–4. https://doi.org/10.1016/S0958-3947(02)00235-2.
[4] Schiapparelli P, Zefiro D, Massone F, Taccini G. Total skin electron therapy (TSET): a reimplementation using radiochromic films and IAEA TRS-398 code of practice. Med Phys 2010;37:3510–7. https://doi.org/10.1118/1.3442301.
[5] Karzmark CJ, Loevinger R, Steele RE, Weissbluth M. A technique for large-field, superficial electron therapy. Radiology 1960;74:633–44. https://doi.org/10.1148/74.4.633.
[6] Koken PW, Murrer LHP. Total body irradiation and total skin irradiation techniques in belgium and the Netherlands: current clinical practice. Adv Radiat Oncol 2021;6:100664. https://doi.org/10.1016/j.adro.2021.100664.
[7] Piotrowski T, Milecki P, Skórska M, Fundowicz D. Total skin electron irradiation techniques: a review. Adv Dermatol Allergol 2013;1:50–5. https://doi.org/10.5114/pdia.2013.33379.
[8] Lastrucci A, Canzani E, Haghighatjou N, Marrazzo L, Iosca N, Wandael Y, et al. Patient positioning and treatment techniques in total skin irradiation: a scoping review. Cancers (Basel) 2025;17. https://doi.org/10.3390/cancers17081276.
[9] Peters VG, Jaywant SM. Implementation of total skin electron therapy using an optional high dose rate mode on a conventional linear accelerator. Med Dosim 1995;20:99–104. https://doi.org/10.1016/0958-3947(95)00013-m.
[10] Ding GX, Osmundson EC, Shinohara ET, Newman NB, Price M, Kirschner AN. Skin dose distributions from total skin electron irradiation therapy (TSET). Int J Radiat Oncol*Biol*Phys 2021;111:e522.
[11] Hensley FW, Major G, Edel C, Hauswald H, Bischof M. Technical and dosimetric aspects of the total skin electron beam technique implemented at Heidelberg University Hospital. Rep Practical Oncol Radiother 2014;19:135–43. https://doi.org/10.1016/j.rpor.2013.07.002.
[12] Baugh G, Al-Alawi T, Fletcher CL, Mills JA, Grieve RJ. A preliminary comparison of total skin electron treatment techniques to demonstrate the application of a mid-torso phantom for measurement of dose penetration. Br J Radiol 2011;84:1125–30. https://doi.org/10.1259/bjr/52924135.
[13] Li R, Tseng W, Wu Q. Validation of the dosimetry of total skin irradiation techniques by Monte Carlo simulation. J Appl Clin Med Phys 2020;21:107–19. https://doi.org/10.1002/acm2.12921.
[14] Shariff M, Stillkrieg W, Lotter M, Lohmann D, Weissmann T, Fietkau R, et al. Dosimetry, Optimization and FMEA of Total Skin Electron Irradiation (TSEI). Z Med Phys 2022;32:228–39. https://doi.org/10.1016/j.zemedi.2021.09.004.
[15] Tandberg DJ, Craciunescu O, Kelsey CR. Radiation therapy for cutaneous T-cell lymphomas. Dermatol Clin 2015;33:703–13. https://doi.org/10.1016/j.det.2015.05.006.
[16] Chowdhary M, Song A, Zaorsky NG, Shi W. Total skin electron beam therapy in mycosis fungoides-a shift towards lower dose? Chin Clin Oncol 2019;8:9. https://doi.org/10.21037/cco.2018.09.02.
[17] Diamantopoulos S, Platoni K, Dilvoi M, Nazos I, Geropantas K, Maravelis G, et al. Clinical implementation of total skin electron beam (TSEB) therapy: a review of the relevant literature. Phys Med 2011;27:62–8. https://doi.org/10.1016/j.ejmp.2010.09.001.
[18] Monzari SF, Geraily G, Aghili M, Toolee H. Evaluation of Dose distribution in optimized stanford total skin electron therapy (TSET) technique in rando anthropomorphic phantom using EBT3 Gafchromatic films. J Biomed Phys Eng 2021. https://doi.org/10.31661/jbpe.v0i0.1035.
[19] Reynard EP, Evans MDC, Devic S, Parker W, Freeman CR, Roberge D, et al. Rotational total skin electron irradiation with a linear accelerator. J Appl Clin Med Phys 2008;9. https://doi.org/10.1120/jacmp.v9i4.2793.
[20] Marrazzo L, Zani M, Pallotta S, Arilli C, Casati M, Compagnucci A, et al. GafChromic® EBT3 films for patient specific IMRT QA using a multichannel approach. Phys Med 2015;31:1035–42. https://doi.org/10.1016/j.ejmp.2015.08.010.
[21] Absorbed Dose Determination in External Beam Radiotherapy. INTERNATIONAL ATOMIC ENERGY AGENCY; 2000. Doi: 10.61092/iaea.ve7q-y94k.
[22] Rogers DWO, Walters B, Kawrakow I. BEAMnrc Users Manual. 2005.
[23] Rogers DWO. Fifty years of Monte Carlo simulations for medical physics. Phys Med Biol 2006;51:R287–301. https://doi.org/10.1088/0031-9155/51/13/R17.
[24] Podgorsak EB, Pla C, Pla M, Lefebvre PY, Heese R. Physical aspects of a rotational total skin electron irradiation. Med Phys 1983;10:159–68. https://doi.org/10.1118/1.595296.
[25] Baehr A, Grohmann M, Platz V, Booken N, Petersen C. Implementing total skin electron irradiation in radiotherapy: a structured change management approach. Strahlenther Onkol 2025. https://doi.org/10.1007/s00066-025-02408-w.
[26] Sarfehnia A, Poon E, Davis SD, Fleming A, Mitchell D, Freeman CR. A novel approach to total skin irradiation using helical TomoTherapy. Pract Radiat Oncol 2014;4:330–5. https://doi.org/10.1016/j.prro.2013.10.004.
[27] Lin C-T, Shiau A-C, Tien H-J, Yeh H-P, Shueng P-W, Hsieh C-H. An attempted substitute study of total skin electron therapy technique by using helical photon tomotherapy with helical irradiation of the total skin treatment: a phantom result. Biomed Res Int 2013;2013:1–7. https://doi.org/10.1155/2013/108794.
[28] Kitaguchi M, Yamashita H, Takenaka R, Okuma K, Nawa K, Nakagawa K. Helical skin radiation therapy including total skin radiation therapy using tomotherapy for primary cutaneous lymphoma with bone marrow suppression as a related adverse event. Pract Radiat Oncol 2021;11:e308–21. https://doi.org/10.1016/j.prro.2020.11.007.
[29] Schaff EM, Rosenberg SA, Olson SJ, Howard SP, Bradley KA. Bone marrow suppression as a complication of total skin helical tomotherapy in the treatment of mycosis fungoides. Radiat Oncol 2018;13:67. https://doi.org/10.1186/s13014-018-1013-2.